



A multi-stage single photochrome system for controlled photoswitching responses

Friedrich Stricker 1, David M. Sanchez 2,3,5, Umberto Raucci 2,3,6, Neil D. Dolinski 4,7, Manuel S. Zayas Jan Meisner 2,3,8, Craig. J. Hawker 1,4, Todd. J. Martínez 2,3 and Javier Read de Alaniz 1,4

The ability of molecular photoswitches to convert on/off responses into large macroscale property change is fundamental to light-responsive materials. However, moving beyond simple binary responses necessitates the introduction of new elements that control the chemistry of the photoswitching process at the molecular scale. To achieve this goal, we designed, synthesized and developed a single photochrome, based on a modified donor-acceptor Stenhouse adduct (DASA), capable of independently addressing multiple molecular states. The multi-stage photoswitch enables complex switching phenomena. To demonstrate this, we show spatial control of the transformation of a three-stage photoswitch by tuning the population of intermediates along the multi-step reaction pathway of the DASAs without interfering with either the first or final stage. This allows for a photonic three-stage logic gate where the secondary wavelength solely negates the input of the primary wavelength. These results provide a new strategy to move beyond traditional on/off binary photochromic systems and enable the design of future molecular logic systems.

he ability to control the properties of a material through the application of external stimuli is of key importance to the ever-growing field of smart materials. Of the stimuli available, light offers numerous attractive features as an external stimulus due to its benign nature, availability and spatial and temporal control¹. To translate the light irradiation into a macroscopic material response, molecular photoswitches that undergo structural changes can be used to enable actuation^{2,3}, control ion conductivity^{4,5} and enhance energy storage^{6,7}. The advancement of these fields has been tightly coupled with structure–property relationship studies of photoswitches that enable a fundamental understanding of their underlying light-driven mechanisms⁸.

In general, photoswitches are converted from the ground-state isomer to the metastable isomer either through a *Z/E* isomerization (for example, of azobenzenes⁹ and hydrazones¹⁰) or a pericyclic reaction (for example, involving diarylethenes^{11,12}, spiropyrans¹³ and dihydroazulenes¹⁴)¹⁵. The reversion back to the original state can be facilitated by a thermal process (T-type) and/or by irradiation with a secondary wavelength (P-type)¹¹, whereas select photoswitches such as azobenzene allow for both (P-/T-type, Fig. 1a)¹. These two-stage photoswitch systems have garnered significant attention for their 'on/off' control, as well as their abilities to represent 0/1 binary digits capable of encoding circuit information.

One strategy to move beyond binary systems and to achieve more complex material responses is to synthetically connect individual photoswitches^{16–18}. Indeed, this approach enables the design of highly functional materials, allowing for multiaddressable systems, increased information storage and complex logic gates^{17,19,20}. However, the challenge is ensuring that the photoswitches retain their intrinsic switching properties while maintaining synthetic

accessibility^{17,20}. A more common approach to increase complexity uses multi-stimuli concepts combining pH changes or electrochemical regulation with light, compromising the spatial and temporal control of light in the second stimulus^{17,18,20}. The development of a single photoswitch capable of selectively addressing metastable intermediates along a multi-step process provides numerous advantages and opens up complex switching phenomena in a single system (Fig. 1b).

Donor–acceptor Stenhouse adducts (DASAs) are a unique class of state-of-the-art visible-light responsive photoswitches that inherently possess such multi-step pathways^{21–23}. In addition, DASA building blocks exhibit a range of desirable material properties such as negative photochromism (that is, photoinduced decolorization and thermal coloration¹⁵), visible-light absorption, polarity switching, high fatigue resistance and a straightforward synthetic route^{24–29}.

However, perhaps the most characteristic property of DASAs is their multi-step photoswitching mechanism that combines an initial actinic Z/E isomerization with several subsequent thermal steps (Figs. 1b and 2)^{21,23,30-34}. Understanding the complex photoswitching mechanism of DASAs has been the topic of a number of experimental^{22,24,25,28,32,35,36} and theoretical studies^{21,33,34,37-39}. The initial actinic Z/E isomerization (from **A** to **B** in Fig. 2) is followed by a bond rotation before the rate-determining 4π -electrocyclization³⁴. The loss of absorbance in the visible region marks the formation of the closed intermediate species **C**, where conjugation along the DASA backbone is lost. Interconversion of this colourless adduct to other tautomeric closed forms (for example, **C**′ to **C**′′′′) is possible and depends on structure and environment^{21,25,35,40}. As a result of this unique step-wise process, the photoswitching of DASA-based

¹Department of Chemistry, UC Santa Barbara, Santa Barbara, CA, USA. ²Department of Chemistry and The PULSE Institute, Stanford University, Stanford, CA, USA. ³SLAC National Accelerator Laboratory, Menlo Park, CA, USA. ⁴Materials Department, Materials Research Laboratory, UC Santa Barbara, Santa Barbara, CA, USA. ⁵Present address: Design Physics Division, Lawrence Livermore National Laboratory, Livermore, CA, USA. ⁶Present address: Italian Institute of Technology, Genova, Italy. ⁷Present address: Pritzker School of Molecular Engineering, University of Chicago, Chicago, IL, USA. ⁸Present address: Heinrich Heine University, Düsseldorf, Germany. [™]e-mail: todd.martinez@stanford.edu; javier@chem.ucsb.edu

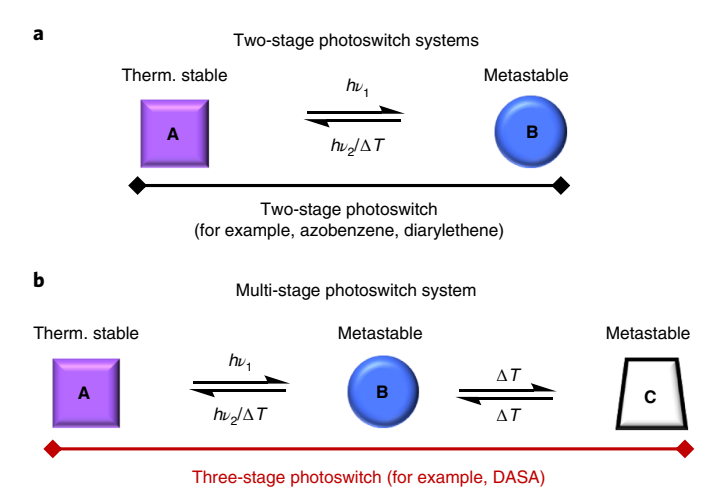


Fig. 1 | Multi-stage photoswitches to move beyond binary systems. **a**, Schematic representation of two-stage photoswitches. **b**, Example of a DASA as a single photochrome multi-stage photoswitch. Herein, 'stage' corresponds to long-lived stable or meta-stable intermediates along the photoswitching pathway that are independently addressable.

systems is initiated by light with subsequent thermal steps governing their overall switching behaviour (property changes).

This multi-step photoswitching mechanism for DASA-based systems (Fig. 2a) has a potential energy surface with several minima and transition states, providing new opportunities to design novel and more complex photomechanical derivatives. Herein, we demonstrate how steric modifications to the DASA moiety can be used to tune this multi-step photoswitching pathway into a system with three independently addressable stages, enabling dual-wavelength control. Herein, 'Stage' corresponds to long-lived stable or meta-stable intermediate(s) along the photoswitching pathway that are independently addressable. We show from the computed potential energy surface and measured reaction kinetics how steric modifications to either the donor or acceptor group can be used to stabilize key intermediates (for example, B and B') along the 4π -electrocyclization pathway. An innovative approach where a second wavelength of light is used to gate the conversion between the actinic and the thermal steps is demonstrated, resulting in a novel three-stage reversible DASA photoswitch. The first stage consists of the isomer A which reacts upon irradiation to the coloured second stage **B**/**B**' exhibiting P-/T-type behaviour. This is followed by the purely thermal 4π -electrocyclization to the third stage which consists of all C isomers. Critically, the second stage involving the **B**/**B**' intermediates can be preferentially addressed via a secondary light stimulus, leading to controlled multi-stage reactivity. This leads to unique characteristics different from two-stage photoswitches. To our knowledge, the behaviour of this negative photochromic three-stage photoswitch cannot be achieved with a traditional two-stage T- or P-type photoswitch. We believe these studies will facilitate the further development of new photoswitches with improved performance and showcases design principles obtained through combined synthesis/computational studies.

Results and discussion

Design of structure–property relationship studies. It has not gone unnoticed that going beyond photoswitches with 'simple' E/Z isomerization or electrocyclization pathways can provide new opportunities to design novel photoswitching properties^{21,35}. Inspired by the work of Buma and Feringa²¹ and guided by computational studies by Martínez and co-workers^{34,41}, we focused on DASA architectures that increase the thermal half-life, stability and population of

B/**B**′ to enable a multi-stage photoswitch by introducing a Stage II (Fig. 2a). Both **B** and **B**′ can be predicted theoretically and observed experimentally by UV–vis spectroscopy, although they are spectroscopically indistinguishable from each other as a transient ~50 nm red-shifted shoulder to the main absorption peak **A** (Fig. 2b)²⁶. Transient absorption experiments below $-40\,^{\circ}$ C demonstrated that irradiation of this shoulder facilitates the reformation of **A** (ref. ³¹). However, previously the lifetimes of **B** and **B**′ were too short-lived to have any practical relevance. To stabilize Stage II (**B**/**B**′, Fig. 2a), we targeted DASA derivatives that decreased the transition rates from **B** to **A** (Stage II to Stage I) and decreased 4π -electrocyclization rates from **B**′ to **C** (Stage II to Stage III, Fig. 2a).

The energy barrier controlling the conversion of B to A (from Stage II to Stage I, Fig. 2a) can be increased by the introduction of a weakly donating arylamine as shown by Buma and co-workers21. Additionally, a destabilization of C (Stage III, Fig. 2a) can be achieved by increasing steric demand on the donor side, effectively shifting the thermodynamic equilibrium in the dark^{21,35}. Unfortunately, in spite of recent synthetic advances³⁶, it is still not possible to synthesize DASA derivatives containing a sterically sufficiently demanding arylamine-derived donor. However, we hypothesized that a similar effect on the triene charge separation can be achieved using steric effects to destabilize the extended donor-acceptor conjugation of A by restricting the formation of the partial double bond in the acceptor ring system (Supplementary Scheme 1), thereby weakening the extended push-pull donor-acceptor conjugation. Furthermore, increasing the steric demand on the donor group should increase the thermodynamic equilibrium from C to A by destabilizing the C intermediates in Stage III.

Building upon these design principles, we generated a library of sterically hindered DASA photoswitches based on previously reported first-generation DASA architectures with new acceptor and donor groups (Fig. 2c). DASA 1 has been investigated previously and consists of a dimethylamine donor and an N,N'-dimethylbarbituric acid acceptor³⁵. DASA 2 was constructed by switching the N,N'-dimethylbarbituric acid acceptor to the more sterically bulky N,N'-(t-butyl)barbituric acid. In addition, we introduced steric demand to the donor side by leveraging an adamantyl-derived amine (Fig. 2c). To investigate the influence of the sterically bulky acceptor and donor moieties, we also synthesized and characterized DASA derivatives by substituting solely the donor (DASA S1) or acceptor groups (DASA S2).

To ensure these substitutions did not interfere with the actinic step, we computed the critical points along the S₁ adiabatic potential energy surface for DASA 1 and DASA 2 (Supplementary Fig. 5). The qualitative features of the potential energy surface for these molecules agree well with our previous Meldrum's acid derived DASA study³⁴. Furthermore, the quantitative agreement between these critical points suggests that steric effects play a small role in the photoisomerization. Steric effects are considered to have the greatest influence on the interconversion between ground-state minima along the ring-closing coordinate. Our previous ab initio dynamical study of DASA ground-state chemistry revealed that most of the isomerizing wavepacket population oscillates in Stage II between B and B', with very little successfully forming Stage III (C isomers, Fig. 2a)41. This is consistent with the relative energies in Fig. 3a and Supplementary Figs. 6, 8 and 9 and previous hypothesis-driven computations that suggest that the ring-closing step from Stage II to Stage III (\mathbf{B}' to \mathbf{C}/\mathbf{C}') is the rate-determining step²⁶. Introducing steric effects into the acceptor and/or donor shifts the relative barrier heights separating these intermediates. The most notable difference is observed in Fig. 3a and Supplementary Figs. 6 and 7, where the thermal reverse reaction to reform Stage I (A, Fig. 2a) plays a significant role in promoting (DASA 1) or impeding (DASA 2) reversion by vibrationally 'hot' B/B' intermediates in Stage II (Fig. 2a). Furthermore, the relative stability of Stage III (C isomers, Fig. 2a),

ARTICLES <u>nature chemistry</u>

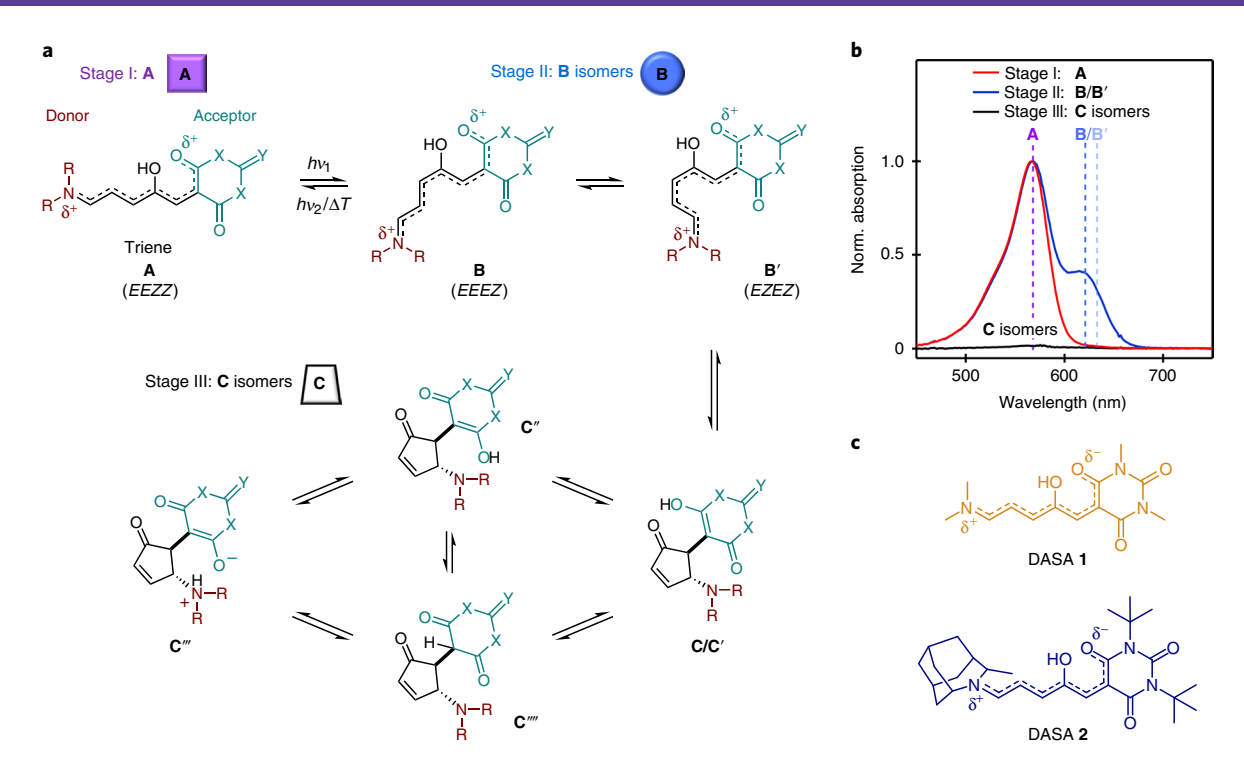


Fig. 2 | A DASA as a single photochrome multi-stage photoswitch. **a**, Schematic representation of the full DASA photoswitching mechanism, which is comprised of three stages: the open-form intermediate **A** (Stage I, violet), the isomerized **B**/**B**′ intermediates (Stage II, blue) and the closed-ring intermediates **C** (Stage III, colourless). **C** and **C**′ differ in the planarization of the donor amine. R, alkyl, aryl; X, N, O; Y, O, Me₂. **b**, Normalized experimental UV-vis spectra of DASA **2** in toluene, showing each stage. Stage II shows a mixture of **A** (λ_{max} = 565 nm) and **B**/**B**′ (λ_{max} = 619 nm) isomers under irradiation with a 530 nm LED. Stage III shows minimal residual absorbance of **A**. The **C** isomers do not absorb in the wavelength range shown. The λ_{max} of the isomers **A** (565 nm), **B** (621 nm) and **B**′ (633 nm) are calculated and shifted from the experimental values by 0.55 eV using the COSMO (ε = 2.38)-ωB97x-D3/def2-TZVP(-f) level of theory and are shown as dashed lines. **c**, Structural modification of sterically hindered dialkylamine DASAs presented in this paper, shown as DASA **1** (yellow) and DASA **2** (blue), respectively. DASA **1** and DASA **2** consist of dimethylamine/*N*, *N*′-dimethylbarbituric acid and adamantyl/*N*,*N*′-(*t*-butyl)barbituric acid donor/acceptor pairs, respectively. DASA **2** directly isomerizes to **C**′ due to the planarization of the nitrogen inside the ring system.

which can shift upwards of 5–6 kcal mol⁻¹ upon the introduction of more sterically hindered acceptor groups, directly influences both the forward and reverse switching rates. This upwards shift is due to steric interactions between the adamantyl and barbituric acid groups after formation of the 4,5-disubstituted cyclopentenone. This interaction results in the rotation of the donor groups for DASAs S2 and 2 compared to DASA 1 (Fig. 3a).

Driven by the design principles suggested from the computed potential energy surfaces, we experimentally analysed the stability of Stage II (B/B') in DASA 2 using DASA 1 as a control (Fig. 3b). In agreement with previous studies, DASA 1 exhibits a high thermodynamic equilibrium (88% open in the dark) and a low solvatochromic shift of -44 nm, suggesting a charge-separated ground state in A (Supplementary Fig. 14 and Supplementary Table 6). The absorbance of DASA 1 in Stage I (A, Fig. 3b) disappears fully upon irradiation, showing the formation of Stage III (C isomers, Fig. 3b). During irradiation, formation of a shoulder representing the B/B' intermediates of Stage II is only transiently observed, quickly funnelling to C (Stage III, Fig. 3b)^{24,35}.

Similar to DASA **1**, DASA **2** exhibits a high thermodynamic equilibrium of >95% open form in the dark while the solvatochromic shift of -17 nm is similar to DASA **S3** (2-methylindoline donor with *N*,*N'*-dimethylbarbituric acid acceptor; -5 nm (ref. ⁴⁰), Supplementary Fig. 14), suggesting an increased hybrid ground-state structure⁴⁰. As a consequence, conjugation along the triene is weakened in DASA **2** compared to DASA **1** (ref. ⁴⁰). Upon irradiation DASA **2** emulates DASA **1**, transforming from Stage I (**A**, Fig. 3b) fully to Stage III (**C** isomers, Fig. 3b) and subsequently

a full recovery to Stage I in the absence of light irradiation, albeit on an extended timescale (8 min versus 1 min from Stage I to Stage III; 700 min versus 60 min for reversal). The extended timescale of the forward reaction can be explained by the high population of Stage II (B/B', Fig. 3b), while the recovery is slower due to the stabilization of C''' and C'''' (Supplementary Figs. 8 and 9) compared to DASA 1. The absorbance of the second Stage II isomers B/B' at 619 nm reaches 40% of the initial absorbance of A before slowly converting into C isomers (Fig. 3b). Furthermore, the lifetime of Stage II is extended in comparison to DASA **S1** with a half-life of 8 s (Supplementary Fig. 21). Previously, this intermediate has only been observed transiently or at low temperature (<-40 °C)²⁶. Consistent with our calculations in Fig. 3a, incorporating the large adamantyl group destabilizes the first isomer in Stage III (C', Fig. 2) while stabilizing B', favouring (kinetically) the thermal recovery to Stage II. Upon extended irradiation, the system can drain towards the thermodynamically more stable Stage III isomers $C^{\prime\prime\prime}$ and $C^{\prime\prime\prime\prime}$, resulting in an overall slower recovery. Furthermore, the N,N'-(t-butyl) barbituric acid acceptor group stabilizes Stage II (B/B', Fig. 2) by increasing the energy barrier of the reverse reaction from **B** to **A**, decreasing the forward and reverse rates of the photoswitching process (Fig. 3a,b). See Supplementary Section 1.12 for an extended discussion and systematic study on the role steric effects play on the overall photoswitching pathway.

Multi-stage photoswitching through a stable B/B' population. Increasing the stability of B/B' while retaining good reversible photoswitching opens up exciting new opportunities for DASA-based

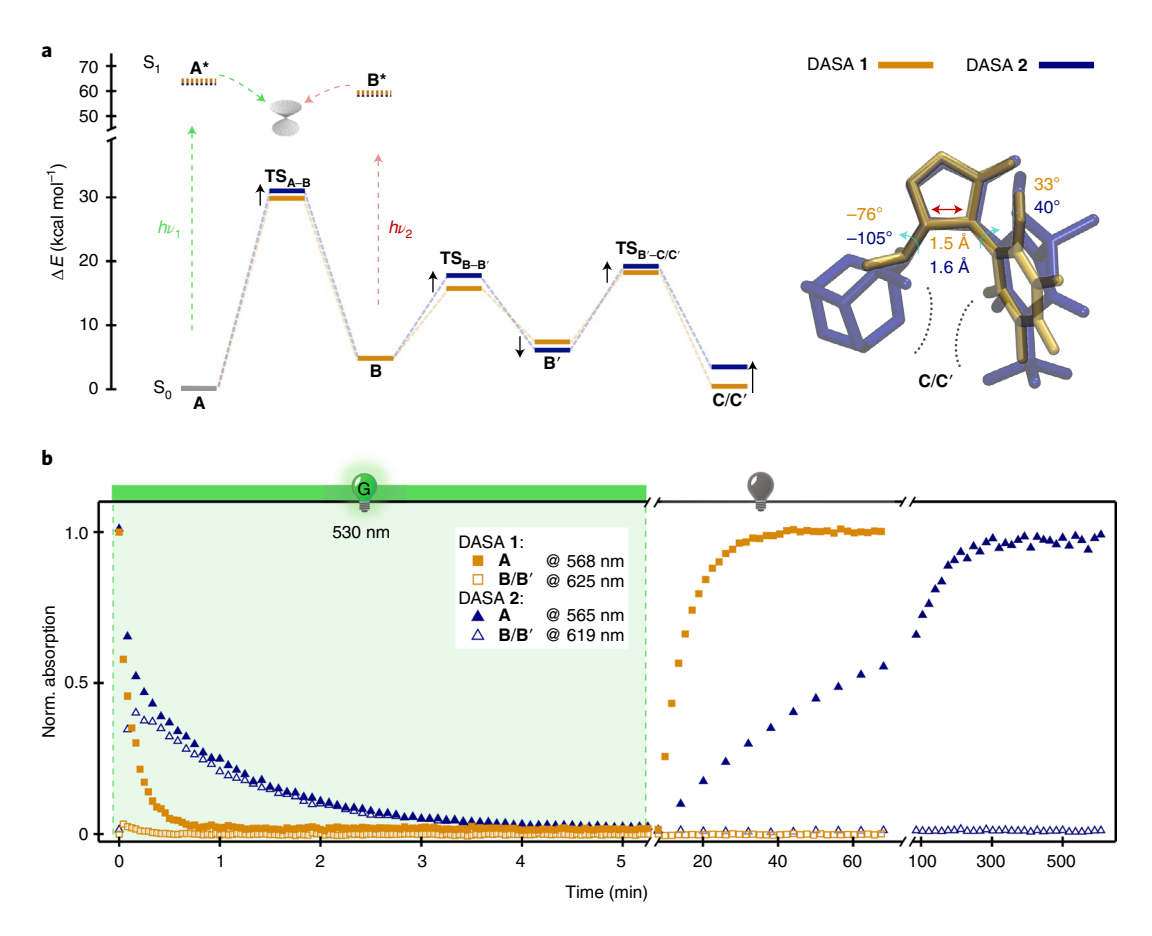


Fig. 3 | Stabilizing Stage II through structural modification in DASA architecture. a, Potential energy surfaces of DASA 1 and DASA 2 for the intermediates up to \mathbf{C}' , including the relevant changes leading to a stabilization of \mathbf{C} computed at the ωB97xD3/def2-TZVP(-f) level of theory in COSMO (ε = 2.38). DASA 2 does not access \mathbf{C} but directly isomerizes to \mathbf{C}' due to the planarization of the nitrogen inside the ring system. The potential energy surface for the full photoswitching mechanism is shown in Supplementary Figs. 6-9. The \mathbf{C}/\mathbf{C}' structures are shown with dihedral angles (°) and C-C bond distances (Å) for DASA 1 (yellow) and DASA 2 (blue). TS, transition state. **b**, Time-dependent UV-vis spectroscopy of DASA 1 and DASA 2 at 10 μM in toluene. The populations of \mathbf{A} and \mathbf{B}/\mathbf{B}' are observed by following their respective λ_{max} during irradiation with a 530 nm LED (indicated by G, 70 mW cm⁻²) for 8 min, and their subsequent recovery in the dark. The results show differences under irradiation and in the thermal recovery in the dark for the two DASAs and the increase in the stability of \mathbf{B}/\mathbf{B}' for DASA 2.

photoswitches (Fig. 4a). The Stage II population shows P-/T-type recovery to Stage I (A, Figs. 2 and 4a) and can be controlled through a secondary wavelength (here 660 nm, Fig. 4a,b). This drives Stage II back to Stage I instead of draining to Stage III. By enabling dual-wavelength control of DASA photoswitches, the intermediate (Stage II) can be addressed through a wavelength which does not interact with either Stage I or Stage III (Fig. 4b). To illustrate this novelty, we first investigated the ability to impart dual-wavelength control by selectively irradiating and suppressing Stage II (B/B', Fig. 4a) with a 660 nm light-emitting diode (LED). This resulted in the reformation of Stage I out of Stage II (A, Fig. 4a), effectively halting access to the closed isomer through a second wavelength of light (Fig. 4c and Supplementary Fig. 25). Molecules already in Stage III (C isomers, Fig. 4a), as expected from lack of absorbance in the visible region, seem not to be affected (Fig. 4c). Furthermore, by controlling the ratio of intensities of the 530 and 660 nm light, we can either slow (for example, by a reduction of the photothermalstationary state (PTSS)—that is, the equilibrium of the light-driven forward reaction and the thermal-driven back reaction⁴²—from 93 to 56%, Supplementary Fig. 27) or effectively halt the forward reaction kinetics directly (Fig. 4c). Interestingly, previously reported molecules, such as DASA 1, show a notably reduced response to a secondary wavelength due to the lower population in Stage II (Supplementary Fig. 28).

The unique ability to set the forward kinetics of the DASA, where the second wavelength of light preferentially interacts with an intermediate along the photoswitching pathway rather than the product, enables new multi-stage photoswitching phenomena (Fig. 5). In non-stirred media, irradiation of negative photoswitches results in a bleaching front at which the photoswitch is transformed from absorbing to non-absorbing and moves through the bulk sample at a fixed rate (Supplementary Fig. 29)43,44. The sample that is passed by the front is fully transformed to the metastable isomer (B for a two-stage photoswitch, C isomers for the DASA) and the untouched sample remains fully in A. The illustrations shown in Fig. 5a,b and Supplementary Fig. 29 depict the benefit of controlling negative photochromic (irradiation leads to loss of absorbance at the excitation wavelength) multi-stage photoswitches in such an environment. The DASA critically showcases negative photochromic properties both in Stage I (A) as well as Stage II (B isomers). This moves beyond what is currently possible with state-of-the-art two-stage photoswitch platforms. The negative photochromic three-stage photoswitch results in a spatially controlled transient population of the photoproduct B (Fig. 5a), addressable through a second wavelength of light at the bleaching front interface, where the first wavelength of light interacts with Stage I, the coloured absorbing species A. The colourless non-absorbing product of the photoreaction, Stage III (C), does not interact with either the first ARTICLES NATURE CHEMISTRY

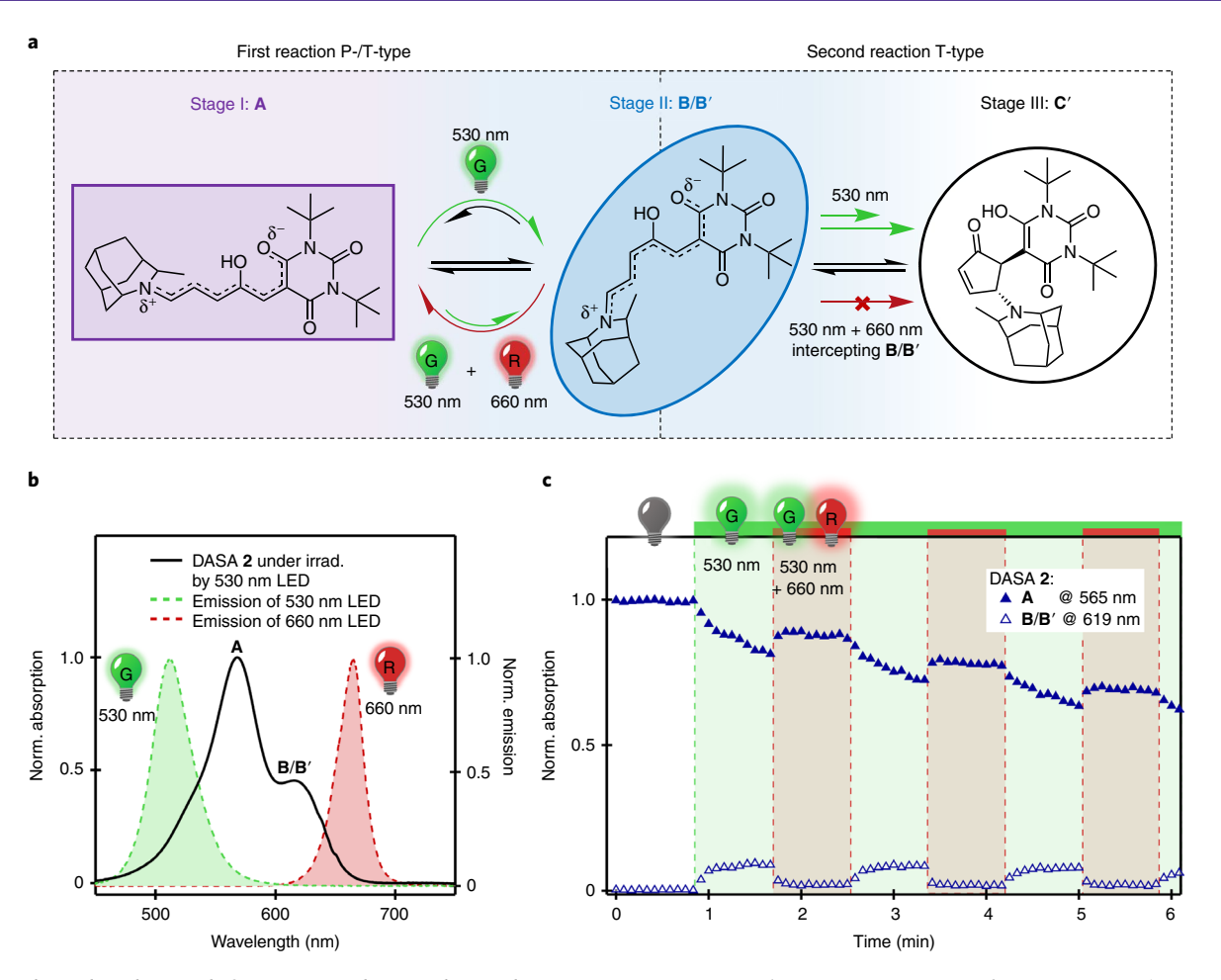


Fig. 4 | Dual wavelength control of DASA 2 switching mechanism by intercepting Stage II. a, Schematic representation of A as Stage I, B/B' as Stage II and C' (and subsequent C isomers) as Stage III. A secondary wavelength can be used to intercept the switching mechanism at Stage II as observed in c. b, Absorption profile of DASA 2 under irradiation showing both molecules in Stage I (A) and Stage II (B/B') and the emission profiles of the 530 and 660 nm LEDs used (indicated by G and R, respectively). c, Time-dependent pump-probe UV-vis spectroscopy of DASA 2 at $10 \,\mu\text{M}$ in toluene showing both A and B/B' intermediates. Transformation of A to C through irradiation with a 530 nm LED (indicated by G, 1.2 mW cm⁻²) can be interrupted by irradiation with a 660 nm LED (indicated by R, 128.0 mW cm⁻²) which promotes conversion of B/B' to A.

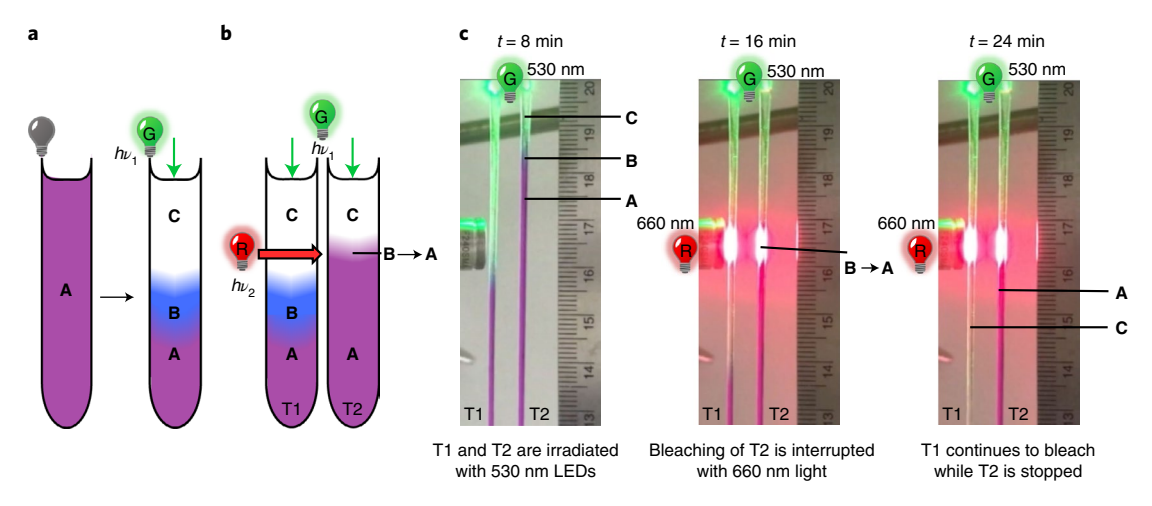


Fig. 5 | Intercepting a transient intermediate allows for advanced control of photoswitch population. a, Irradiation of a negative three-stage photoswitch leads to a thin layer of the transient intermediate **B** as seen in Supplementary Video 1. **b**, In a negative three-stage photoswitch, perpendicular irradiation can be used to selectively stop the transformation from **A** to **C** through a volume filled with either **A** or **C** as seen in Supplementary Video 5 and **c**, while in a typical two-stage P-type photoswitch the $h\nu_2$ interacts with **B** and will get absorbed if passing through a volume filled with bleached sample. **c**, Photographic stills of Supplementary Video 5 showing how 660 nm light can be used to stop the transformation from **A** to **C** in a secondary glass tube (T2) under constant irradiation with 530 nm light through a glass tube (T1) containing already converted DASA **2** in isomer **C**. G indicates a 530 nm LED (green light, 1 mW) and R indicates a 660 nm LED (red light, 73 mW). Units of the rulers shown are in cm.

or secondary wavelength, allowing for an interaction with Stage II (**B**) through volumes of Stage I and Stage III (Fig. 5b). In traditional dual-wavelength controlled photoswitches, such as diarylethene or azobenzene, the second wavelength of light interacts with the product from the photoisomerization process, driving the reaction back to the original state (that is, on/off control of the two-stage photoisomerization reaction) (Supplementary Fig. 29).

To highlight the more complex photoswitching phenomena enabled by negative photochromic three-stage switching pathways, we first demonstrated that the transient population of the photoproduct B/B' in Stage II can be seen with the naked eye upon irradiation with 530 nm light (Fig. 5a and Supplementary Video 1). Using a fibre-optic splitter that allows 530 and 660 nm light to be delivered from the top of the sample in parallel or individually enables control of the switching-front depth (Supplementary Fig. 29 and Supplementary Video 2). Continued irradiation with 530 nm or white light drives the reaction to Stage III in the regions not exposed to 660 nm light (Supplementary Videos 3 and 4 and Supplementary Fig. 31). By setting the 660 nm LED perpendicular to the bleaching front, we can arrest the reaction at a set distance (Supplementary Video 4) by interrupting Stage II. While fundamentally controlling a photostationary state and a bleaching front with a second wavelength of light could be achieved with a two-stage P-type photoswitch, it would be extremely challenging and require judicious choice of a negative photoswitch coupled with a precise understanding of the photoswitching kinetics.

Finally, to demonstrate true novelty, we set up two glass tubes with DASA 2 in toluene and a 530 nm LED on the top and a perpendicular 660 nm LED. Unique to this negative photochromic three-stage photoswitch is the fact that the secondary wavelength (660 nm) does not interact with the photoproduct in Stage III, which is transparent. This enables light to pass freely through the closed isomers C through C''' in Stage III in the first tube and selectively stop the bleaching front in the neighbouring glass tube T2 (Fig. 5a,b and Supplementary Video 5). While simultaneously controlling the bleaching front in tube T2, the photochromic switching process in tube T1 is uninterrupted, enabling a continuous bleaching of DASA 2. This represents a photonic three-stage logic gate where the secondary wavelength solely negates the input of the primary wavelength. A similar experiment with a two-stage P-type photoswitch such as diarylethenes or azobenzenes would lead to a reversion of the photoproduct upon irradiation with the second wavelength of light in the tube T1, thereby blocking light penetration and preventing control of the photoswitching process. We believe the selective interaction with the metastable intermediate B/B' in Stage II without interfering with the photoproducts C through C''' in Stage III will enable a number of exciting new applications where more complex switching phenomena are desired, such as logic gates and additive manufacturing⁴⁵. Isolating isomers along the reaction pathway of other multi-step photoswitches such as spiropyrans or increasing the number of separate stages in multi-stage photoswitches will further enrich the toolbox for light-responsive smart materials.

Conclusion

Using the powerful insight from both computation and synthesis we developed DASA-based photochromic compounds with steric demand on both the donor and acceptor groups that enable a controlled three-stage single photochrome photoswitching system. Computed reaction pathways and pump-probe UV-vis spectroscopy together with NMR spectroscopy serve to explain the influence each modification has on the light-responsive behaviour, mainly focusing on the key intermediates B/B' and C/C'. This work showcases the relationship between steric effects and photoswitching properties and the potential to move beyond simple two-stage photoswitches. Through the design insights from these studies, we demonstrate a dual-wavelength responsive DASA by selectively

intercepting the metastable intermediate B/B' and reverting it to **A**. This introduces a P-/T-type step which is directly followed by a thermal step enabling a negative photochromic three-stage photoswitch where the intermediate in Stage II, not the photoproduct in Stage III, is selectively addressed with a second wavelength of light. Indeed, the extent of this effect depends on the population of intermediates in Stage II and the ratio of intensities between the primary and secondary light source. This allows for spatial control of the transformation through samples containing either the stable isomer A or the metastable closed form in Stage III, which is not possible with previously reported two-stage photoswitches. By coupling synthesis and computation, a detailed understanding of the energy landscape and lifetimes of key intermediates leads to the design of a novel switching mechanism and associated photochromic properties for DASA derivatives. Significantly, these advances and principles are not restricted to a narrow subset of materials and support the development of new multi-stage photoswitches.

Online content

Any methods, additional references, Nature Research reporting summaries, source data, extended data, supplementary information, acknowledgements, peer review information; details of author contributions and competing interests; and statements of data and code availability are available at https://doi.org/10.1038/s41557-022-00947-8.

Received: 2 September 2021; Accepted: 7 April 2022; Published online: 9 June 2022

References

- Feringa, B. L. & Browne, W. R. (eds) Molecular Switches 2nd edn, Vol. 1 (Wiley-VCH Verlag GmbH & Co. KGaA, 2011).
- Iamsaard, S. et al. Conversion of light into macroscopic helical motion. Nat. Chem. 6, 229–235 (2014).
- Li, J., Zhou, X. & Liu, Z. Recent advances in photoactuators and their applications in intelligent bionic movements. *Adv. Opt. Mater.* 8, 2000886 (2020).
- Soberats, B. et al. Macroscopic photocontrol of ion-transporting pathways of a nanostructured imidazolium-based photoresponsive liquid crystal. *J. Am. Chem. Soc.* 136, 9552–9555 (2014).
- Nie, H. et al. Light-controllable ionic conductivity in a polymeric ionic liquid. Angew. Chem. Int. Ed. 59, 5123–5128 (2020).
- Qiu, Q., Shi, Y. & Han, G. G. D. Solar energy conversion and storage by photoswitchable organic materials in solution, liquid, solid, and changing phases. J. Mater. Chem. C 9, 11444–11463 (2021).
- Goulet-Hanssens, A., Eisenreich, F. & Hecht, S. Enlightening materials with photoswitches. Adv. Mater. 32, 1905966 (2020).
- Browne, W. R. & Feringa, B. L. Making molecular machines work. Nat. Nanotechnol. 1, 25–35 (2006).
- Bandara, H. M. D. & Burdette, S. C. Photoisomerization in different classes of azobenzene. Chem. Soc. Rev. 41, 1809–1825 (2012).
- Su, X. & Aprahamian, I. Hydrazone-based switches, metallo-assemblies and sensors. Chem. Soc. Rev. 43, 1963–1981 (2014).
- Irie, M. Diarylethenes for memories and switches. Chem. Rev. 100, 1685–1716 (2000).
- Irie, M., Fukaminato, T., Matsuda, K. & Kobatake, S. Photochromism of diarylethene molecules and crystals: memories, switches, and actuators. *Chem. Rev.* 114, 12174–12277 (2014).
- Minkin, V. I. Photo-, thermo-, solvato-, and electrochromic spiroheterocyclic compounds. Chem. Rev. 104, 2751–2776 (2004).
- Daub, J., Knöchel, T. & Mannschreck, A. Photosensitive dihydroazulenes with chromogenic properties. Angew. Chem. Int. Ed. 23, 960–961 (1984).
- Bouas-Laurent, H. & Dürr, H. Organic photochromism. Pure Appl. Chem. 73, 639–665 (2001).
- Mrozek, T., Görner, H. & Daub, J. Towards multifold cycloswitching of biphotochromes: investigation on a bond-fused dihydroazulene/ vinylheptafulvene and dithienylethene/dihydrothienobenzothiophene. Chem. Commun.1487–1488 (1999).
- Fihey, A., Perrier, A., Browne, W. R. & Jacquemin, D. Multiphotochromic molecular systems. *Chem. Soc. Rev.* 44, 3719–3759 (2015).
- Nie, H., Self, J. L., Kuenstler, A. S., Hayward, R. C. & Read de Alaniz, J. Multiaddressable photochromic architectures: from molecules to materials. Adv. Opt. Mater. 7, 1900224 (2019).

ARTICLES NATURE CHEMISTRY

- Perrier, A., Maurel, F. & Jacquemin, D. Single molecule multiphotochromism with diarylethenes. Acc. Chem. Res. 45, 1173–1182 (2012).
- Andréasson, J. & Pischel, U. Light-stimulated molecular and supramolecular systems for information processing and beyond. *Coord. Chem. Rev.* 429, 213695 (2021).
- Zulfikri, H. et al. Taming the complexity of donor-acceptor Stenhouse adducts: infrared motion pictures of the complete switching pathway. *J. Am. Chem. Soc.* 141, 7376–7384 (2019).
- Mallo, N. et al. Hydrogen-bonding donor-acceptor Stenhouse adducts. ChemPhotoChem 4, 407–412 (2020).
- Lerch, M. M., Szymański, W. & Feringa, B. L. The (photo)chemistry of Stenhouse photoswitches: guiding principles and system design. *Chem. Soc. Rev.* 47, 1910–1937 (2018).
- Helmy, S. et al. Photoswitching using visible light: a new class of organic photochromic molecules. J. Am. Chem. Soc. 136, 8169–8172 (2014).
- Mallo, N. et al. Photochromic switching behaviour of donor-acceptor Stenhouse adducts in organic solvents. Chem. Commun. 52, 13576–13579 (2016).
- Lerch, M. M., Wezenberg, S. J., Szymanski, W. & Feringa, B. L. Unraveling the photoswitching mechanism in donor–acceptor Stenhouse adducts. *J. Am. Chem. Soc.* 138, 6344–6347 (2016).
- Lerch, M. M. et al. Tailoring photoisomerization pathways in donor-acceptor Stenhouse adducts: the role of the hydroxy group. *J. Phys. Chem. A* 122, 955–964 (2018).
- Hemmer, J. R. J. R. et al. Controlling dark equilibria and enhancing donor-acceptor Stenhouse adduct photoswitching properties through carbon acid design. J. Am. Chem. Soc. 140, 10425–10429 (2018).
- Hemmer, J. R. et al. Tunable visible and near infrared photoswitches. J. Am. Chem. Soc. 138, 13960–13966 (2016).
- Lerch, M. M., Hansen, M. J., Velema, W. A., Szymanski, W. & Feringa, B. L. Orthogonal photoswitching in a multifunctional molecular system. *Nat. Commun.* 7, 12054 (2016).
- Di Donato, M. et al. Shedding light on the photoisomerization pathway of donor-acceptor Stenhouse Adducts. J. Am. Chem. Soc. 139, 15596–15599 (2017).
- Lerch, M. M. et al. Solvent effects on the actinic step of donor-acceptor Stenhouse adduct photoswitching. Angew. Chem. Int. Ed. 57, 8063–8068 (2018).
- Laurent, A. D., Medved, M. & Jacquemin, D. Using time-dependent density functional theory to probe the nature of donor-acceptor Stenhouse adduct photochromes. *ChemPhysChem* 17, 1846–1851 (2016).

- Sanchez, D. M., Raucci, U., Ferreras, K. N. & Martínez, T. J. Putting photomechanical switches to work: an ab initio multiple spawning study of donor-acceptor Stenhouse adducts. J. Phys. Chem. Lett. 11, 7901–7907 (2020).
- 35. Mallo, N. et al. Structure-function relationships of donor-acceptor Stenhouse adduct photochromic switches. *Chem. Sci.* **9**, 8242–8252 (2018).
- Clerc, M. et al. Promoting the furan ring opening reaction to access new donor-acceptor Stenhouse adducts with hexafluoroisopropanol. *Angew. Chem. Int. Ed.* 60, 10219–10227 (2021).
- García-Iriepa, C., Marazzi, M. & Sampedro, D. From light absorption to cyclization: structure and solvent effects in donor-acceptor Stenhouse adducts. *ChemPhotoChem* 3, 866–873 (2019).
- García-Iriepa, C. & Marazzi, M. Level of theory and solvent effects on DASA absorption properties prediction: comparing TD-DFT, CASPT2 and NEVPT2. *Materials* 10, 1025 (2017).
- Berraud-Pache, R. et al. Redesigning donor-acceptor Stenhouse adduct photoswitches through a joint experimental and computational study. *Chem. Sci.* 12, 2916–2924 (2021).
- Sroda, M. M., Stricker, F., Peterson, J. A., Bernal, A. & Read de Alaniz, J. Donor-acceptor Stenhouse adducts: exploring the effects of ionic character. Chem. Eur. J. 27, 4183–4190 (2020).
- Sanchez, D. M., Raucci, U. & Martínez, T. J. In silico discovery of multistep chemistry initiated by a conical intersection: the challenging case of donor–acceptor Stenhouse adducts. *J. Am. Chem. Soc.* 143, 20015–20021 (2021).
- Stranius, K. & Börjesson, K. Determining the photoisomerization quantum yield of photoswitchable molecules in solution and in the solid state. *Sci Rep.* 7, 41145 (2017).
- 43. Terrones, G. & Pearlstein, A. J. Effects of optical attenuation and consumption of a photobleaching initiator on local initiation rates in photopolymerizations. *Macromolecules* **34**, 3195–3204 (2001).
- 44. Dolinski, N. D. et al. A versatile approach for in situ monitoring of photoswitches and photopolymerizations. *ChemPhotoChem* 1, 125–131 (2017).
- Dolinski, N. D. et al. Solution mask liquid lithography (SMaLL) for one-step, multimaterial 3D printing. Adv. Mater. 30, 1800364 (2018).

Publisher's note Springer Nature remains neutral with regard to jurisdictional claims in published maps and institutional affiliations.

© The Author(s), under exclusive licence to Springer Nature Limited 2022

Methods

Time-dependent UV-vis spectroscopy. The photoinduced optical absorption kinetics were measured on a pump-probe setup. The pump beam was generated by an LED source (Thorlabs) coupled into a multimode optical fibre terminated with an output collimator. The LED intensity was controlled through a digital-to-analogue converter (National Instruments USB-6009) using LabVIEW. The probe beam was produced by a High Power MINI Deuterium Tungsten Halogen Source with a 200-2,000 nm shutter (Ocean Optics DH-MINI) coupled into a multimode fibre-optic cable with an output collimator for the light delivery. The probe light was modulated by a shutter (Uniblitz CS25) which could be controlled manually or through a digital output port (National Instruments USB-6009) using LabVIEW. Pump and probe beams were overlapped using steering and focusing optics at a 90° angle inside a sample holder, which allowed for 10×10 mm rectangular spectrophotometer cells that were connected to a circulating bath for temperature control. Additionally, the solutions were stirred during the measurements using a miniature stirring plate inserted into the sample holder (Starna Cells SCS 1.11). The probe beam was collected through a system of lenses in the detector (Ocean Optics Flame-S1-XR spectrometer). The detector was connected to a PC via USB port and controlled by a National Instrument LabVIEW program. Experiments were performed at $10\,\mu M$ concentration unless otherwise stated. Samples were left to equilibrate overnight prior to the measurements unless otherwise stated.

Minimum energy pathway calculations. We employed GPU-accelerated complete active space self-consistent field theory (SA-CASSCF)⁴⁶⁻⁴⁸ and density functional theory (DFT) to study the complete photoswitching pathway for a series of first generation sterically hindered DASAs (Fig. 2). All electronic structure calculations (that is, energies, gradients and non-adiabatic coupling vectors (NACV)) were performed with the TeraChem⁴⁹⁻⁵¹ electronic structure package.

To characterize the actinic step of these novel DASA derivatives, critical points (for example, the Frank–Condon point (FC), S_1 minimum and S_1/S_0 minimum energy conical intersections (MECI) for α and β along the isomerization pathways) were computed using the DL-FIND (ref. 52) optimization package. We used an active space consisting of two electrons in two orbitals determined to minimize the average energy of the lowest three singlet states, in conjunction with the 6-31G** basis set (that is, SA3-CAS(2,2)SCF/6-31G**). Cartesian coordinates, energies, CI vectors and CASSCF natural orbitals are included in Supplementary Sections 1.4 and 1.10.

To characterize the thermal step, geometries were optimized on the electronic ground state at the $\omega B97x$ -D3/def2-TZVP(-f) level of theory using the equilibrium COnductor-like Screening MOdel (COSMO) to incorporate the polarization of the toluene environment (ε =2.38). Transition states were computed from converging the climbing image from minimum energy pathways using the Dimer method³³ in ChemShell³⁴, ⁵⁵ (see Supplementary Section 1.4 for computational protocol). The Hessian was determined to be positive definite at the observed minimum (that is, all frequencies were positive), while at the transition state it possessed one negative eigenvalue (that is, a single imaginary frequency) along the direction connecting the two minima (that is, reactant and product). Geometries and energies for minima and transition states along with videos constructed from these structures are included in the supplementary files.

Data availability

All data (experimental procedures and characterization data) supporting the findings of this study are available within the Article and its Supplementary Information. Source data are provided with this paper.

Code availability

The codes used for the analysis of the raw experimental and simulation data and for the generation of the manuscript figures are available from the corresponding authors upon request.

References

- Hohenstein, E. G., Luehr, N., Ufimtsev, I. S. & Martínez, T. J. An atomic orbital-based formulation of the complete active space self-consistent field method on graphical processing units. J. Chem. Phys. 142, 224103 (2015).
- Snyder, J. W., Curchod, B. F. E. & Martínez, T. J. GPU-accelerated state-averaged complete active space self-consistent field interfaced with ab initio multiple spawning unravels the photodynamics of provitamin D₃. J. Phys. Chem. Lett. 7, 2444–2449 (2016).
- 48. Snyder, J. W., Fales, B. S., Hohenstein, E. G., Levine, B. G. & Martínez, T. J. A direct-compatible formulation of the coupled perturbed complete active space self-consistent field equations on graphical processing units. *J. Chem. Phys.* 146, 174113 (2017).
- Ufimtsev, I. S. & Martinez, T. J. Strategies for two-electron integral evaluation. J. Chem. Theory Comput. 4, 222–231 (2008).
- Ufimtsev, I. S. & Martinez, T. J. Quantum chemistry on graphical processing units. 2. Direct self-consistent-field implementation. *J. Chem. Theory Comput.* 5, 1004–1015 (2009).
- Ufimtsev, I. S. & Martinez, T. J. Quantum chemistry on graphical processing units. 3. Analytical energy gradients, geometry optimization, and first principles molecular dynamics. J. Chem. Theory Comput. 5, 2619–2628 (2009).
- Kästner, J. et al. DL-FIND: an open-source geometry optimizer for atomistic simulations. J. Phys. Chem. A 113, 11856–11865 (2009).
- Henkelman, G. & Jónsson, H. A dimer method for finding saddle points on high dimensional potential surfaces using only first derivatives. *J. Chem. Phys.* 111, 7010–7022 (1999).
- 54. ChemShell: A Computational Chemistry Shell; www.chemshell.org
- Sherwood, P. et al. QUASI: A general purpose implementation of the QM/MM approach and its application to problems in catalysis. J. Mol. Struc. (Theochem.) 632, 1–28 (2003).

Acknowledgements

This research reported here was supported by the Office of Naval Research through the MURI of Photomechanical Materials Systems (ONR N00014-18-1-2624). F.S. thanks the German National Academic foundation for an ERP-Fellowship. N.D.D. was supported by the Institute for Collaborative Biotechnologies under Contract Number W911NF-09-D-00010. D.M.S. is grateful to the National Science Foundation for a graduate fellowship. Lawrence Livermore National Laboratory is operated by Lawrence Livermore National Security, LLC, for the US Department of Energy, National Nuclear Security Administration under Contract DE-AC52-07NA27344. The authors acknowledge the use of the NSF (grant no. MRI-1920299) for the acquisition of Bruker 500 MHz and 400 MHz NMR instruments. We also want to thank K. Culhane for the table-of-contents graphic.

Author contributions

The project was conceptualized by F.S., N.D.D. and J.R.d.A. while the experimental design and methodology were developed by F.S., D.M.S., U.R. and N.D.D. The experiments were conducted by F.S., N.D.D. and M.S.Z. while D.M.S., U.R., J.M. and T.J.M. performed the ab initio simulations. The data were analysed by F.S., D.M.S., U.R., N.D.D., J.M., T.J.M. and J.R.d.A. The project was supervised by T.J.M. and J.R.d.A. The manuscript was written by F.S., D.M.S., U.R. and J.R.d.A. and edits were conducted by all authors.

Competing interests

The authors declare no competing interests.

Additional information

Supplementary information The online version contains supplementary material available at https://doi.org/10.1038/s41557-022-00947-8.

Correspondence and requests for materials should be addressed to Todd. J. Martínez or lavier Read de Alaniz.

Peer review information *Nature Chemistry* thanks Michael Lerch, Helena Shepherd and Brian Wagner for their contribution to the peer review of this work.

Reprints and permissions information is available at www.nature.com/reprints.